Semi-Lagrangian simulations on polar grids: from diocotron instability to ITG turbulence

Nicolas Crouseilles, Pierre Glanc, Sever Adrian Hirstoaga, Eric Madaule, Michel Mehrenberger, Jérôme Pétri

EPJ manuscript No.
(will be inserted by the editor)

Semi-Lagrangian simulations on polar grids: from diocotron instability to ITG turbulence

Nicolas Crouseilles[1], Pierre Glanc[2], Sever Hirstoaga[2], Eric Madaule[3], Michel Mehrenberger[2,4] and Jérôme Pétri[5]

[1] INRIA-Rennes (IPSO team) & IRMAR, Rennes, France
[2] INRIA-Nancy (TONUS team) & IRMA, Strasbourg, France
[3] Institut Jean Lamour, Nancy, France
[4] Max-Planck-Institut für Plasmaphysik, Garching, Germany
[5] IRMA, Université de Strasbourg, France
[6] Observatoire Astronomique de Strasbourg, Strasbourg, France

Received: date / Revised version: date

Abstract. While developing a new semi-Lagrangian solver, the gap between a linear Landau run in $1D \times 1D$ and a $5D$ gyrokinetic simulation in toroidal geometry is quite huge. Intermediate test cases are welcome for checking the code. We consider here as building block, a $2D$ guiding center type equation on an annulus. We first revisit a $2D$ test case previously done with a PIC approach [15] and detail the boundary conditions. We then consider a $4D$ drift kinetic slab simulation [10] for which we give some first results of a new conservative method.

PACS. PACS-key discribing text of that key – PACS-key discribing text of that key

1 Introduction

Kinetic models are known to be a precise tool to describe plasma arising in tokamak or in beam. However, this accurate description requires an important effort in terms of numerics, since the solution of a kinetic model depends not only on the space variable, but also on the velocity variable, which makes a six dimensional phase space. In addition to the filamentation phenomena and presence of small scales, the numerical approximation of the distribution function solution to the kinetic model is a huge challenge despite the increase of nowadays computers power.

In the last decades, several different numerical methods have been developed to this aim. Among them, the Particle In Cell (PIC) exploits the Lagrangian formulation of the kinetic equation by solving the characteristics equations. In spite of its relative low computational cost, these kinds of method suffer from unaccuracy in low density regions and low convergence rate when the number of macro-particles increases (see [1]). On the other side, Eulerian methods have been introduced. They are based on methods such that finite volumes or finite differences methods mostly developed in fluids mechanics; the main particularity is that they require a grid of the full phase space which makes them accurate independently of the value of the distribution function, but they are very costly in terms of memory and computational cost. Moreover, a restriction on the time step has to be satisfied for stability reasons. An interesting compromise is the semi-Lagrangian method which tries to take benefit from the Lagrangian approach by tracking the time evolution of the characteristic equations of the kinetic model, and from the Eulerian framework by using a grid of the phase space. In particular, the so-obtained method is free from standard CFL conditions on the time step.

Different semi-Lagrangian methods have been developed over this last 40 years [8], [2], [17], to first compute the solution of the $1D \times 1D$ Vlasov-Poisson equation and then of the guiding-center model and more recently of the $5D$ gyrokinetic model. In addition to the high dimensionality, the spatial geometry of the latter case is toroidal, which makes it more complicated to deal with.

While developing a new semi-Lagrangian solver, the gap between a linear Landau run obtained with the $1D \times 1D$ Vlasov-Poisson model and a $5D$ gyrokinetic simulation in toroidal geometry is quite huge. Then, intermediate test cases are welcome for checking the performance and precision of the codes.

Tests for which the analytical solution is known at all times do not include usually sufficient complexity to tackle the difficulties of the final problem. Moreover, although interesting, some test cases are not published and often different parameter settings are chosen which makes difficult cross validations with different schemes. Then, a purpose of this work is to provide precise parameter setting for two test cases which have intermediate complexity between analytic test and realistic physical configuration.

We consider here as building block, a $2D$ guiding center type equation on an annulus satisfied by $f(t,r,\theta)$:

$$\partial_t f - \frac{\partial_\theta \Phi}{r}\partial_r f + \frac{\partial_r \Phi}{r}\partial_\theta f = 0,\ t \in [0,T], \tag{1}$$

with $(r,\theta) \in \Omega = [r_{\min}, r_{\max}]\times[0,2\pi]$, where the potential Φ solves a Poisson type equation. This model constitutes the basis of the two tests. We first revisit a $2D$ test case previously done with a PIC approach [15] and detail the boundary conditions. We then consider a $4D$ drift kinetic slab simulation [10], [4] which can be viewed as a polar guiding-center equation of type (1) coupled with a Vlasov type equation in the parallel (z,v) direction.

In this latter case, some first results of a new conservative semi-Lagrangian method are given and compared the standard one [10]. Indeed, it is well known that the BSL method does not preserve the total mass exactly in the $2D$ general configuration. Then, in the spirit of [6], we propose a conservative semi-Lagrangian method. More precisely, a generalization to the $2D$ case of [6] is presented in this work to deal with model of the form (1) without considering directional splitting. Indeed, even if time splitting techniques are very efficient in the Vlasov-Poisson case, for drift-kinetic or guiding-center models considered here, the characteristic curves are more complicated and need to be tackle in the full $2D$ case. Hence, to overcome the lack of conservation of the standard BSL method, it seems interesting to develop, validate and compare a $2D$ conservative semi-Lagrangian method. Let us remark that similar motivations are considered in [18].

The rest of this work is organized as follows: first, the diocotron instability test case [15] is revisited by detailing the radial boundary conditions and the associated instability rates. The following section is devoted to the presentation of a $4D$ drift-kinetic test case. In sections 4 and 5, the standard semi-Lagrangian method and the new conservative semi-Lagrangian method are proposed. Finally numerical results will be shown in the last section.

2 Diocotron instability test case

We consider $\rho(t,r,\theta)$, solution of (1), with $\Phi(t,r,\theta)$ solving Poisson equation:

$$-\partial_r^2\Phi - \frac{1}{r}\partial_r\Phi - \frac{1}{r^2}\partial_\theta^2\Phi = \gamma\rho, \tag{2}$$

where $\gamma \in \{-1,1\}$, depending on the context (astrophysic or plasma physics). The guiding-center model (1)-(2) satisfied by $\rho(t,r,\theta)$ is associated to an initial condition $\rho(t=0,r,\theta)$ (see [7])

$$\rho(t=0,r,\theta) = \begin{cases} 0,\ r_{\min} \le r < r^-, \\ 1+\epsilon\cos(\ell\theta),\ r^- \le r \le r^+, \\ 0,\ r^+ < r \le r_{\max}, \end{cases}$$

where $\epsilon = 10^{-6}$. We also need to define boundary conditions. In the $\theta \in [0,2\pi]$ direction, periodic boundary conditions are used so that a Fourier transform is applied to (2) whereas different conditions will be considered in the radial $r \in [r_{\min}, r_{\max}]$ direction. We recall the notation $\Omega = [r_{\min}, r_{\max}] \times [0,2\pi]$.

2.1 Radial boundary conditions for Φ

In this subsection, different radial boundary conditions are proposed to solve (2). In particular, their influence on the conservation of the electric energy

$$\mathcal{E}(t) = \int_\Omega r|\partial_r\Phi|^2 + \frac{1}{r}|\partial_\theta\Phi|^2 dr d\theta, \tag{3}$$

and on the total mass

$$\mathcal{M}(t) = \int_\Omega r\rho dr d\theta, \tag{4}$$

is discussed.

First, homogeneous Dirichlet boundary condition are imposed at $r_{\max}$:

$$\Phi(t, r_{\max}, \theta) = 0, \forall t \ge 0, \theta \in [0,2\pi].$$

Second, at $r_{\min}$, we consider two kinds of boundary conditions. We take either homogeneous Dirichlet boundary condition

$$\Phi(t, r_{\min}, \theta) = 0, \forall t \ge 0, \theta \in [0,2\pi].$$

or the following condition, named Neumann mode 0:

- homogeneous Neumann boundary condition at $r_{\min}$ for the Fourier mode 0 in θ ($\partial_r\widehat{\Phi}_0(t, r_{\min}) = 0$)

$$\int_0^{2\pi} \partial_r\Phi(t, r_{\min}, \theta)d\theta = 0,$$

- homogeneous Dirichlet boundary condition at $r_{\min}$ for the other Fourier modes ($\widehat{\Phi}_k(t, r_{\min}) = 0, \forall k \ne 0$)

$$\Phi(t, r_{\min}, \theta) = \frac{1}{2\pi}\int_0^{2\pi} \Phi(t, r_{\min}, \theta')d\theta'.$$

For this two choices of radial boundary conditions, one can prove (see [13]) that the electric energy and the total mass are preserved in time

$$\partial_t\mathcal{E}(t) = \partial_t\mathcal{M}(t) = 0,$$

which provide a good indicator to compare and validate the numerical methods. A last configuration has been also explored, in which homogeneous Neumann boundary conditions are imposed for all the modes $\partial_r\widehat{\Phi}_k(t, r_{\min}) = 0, \forall k$. Let us remark that however in this case, the electric energy and the total mass are not preserved with time at the continuous level (see [13]).

For the solution ρ, Dirichlet type boundary conditions are considered:

$$\rho(t, r \le r_{\min}, \theta) = \rho(t, r_{\min}, \theta),$$
$$\rho(t, r \ge r_{\max}, \theta) = \rho(t, r_{\max}, \theta).$$

2.2 Instability rates

In this subsection, the instability rates are computed from the linearized problem, considering the different radial boundary conditions.

Considering a radial equilibrium $(n_0(r), \Phi_0(r))$ of (1)-(2) linked by the Poisson equation

$$-\partial_r(r\partial_r\Phi_0) = rn_0,$$

we then search for an approximate solution of (1)-(2) of the form

$$\rho(t,r,\theta) \simeq n_0(r) + \epsilon\widehat{n}_{1,\ell}(r)\exp(\mathrm{i}\ell\theta)\exp(-\mathrm{i}\omega t/\gamma)$$
$$\Phi(t,r,\theta) \simeq \gamma\Phi_0(r) + \epsilon\gamma\widehat{\Phi}_{1,\ell}(r)\exp(\mathrm{i}\ell\theta)\exp(-\mathrm{i}\omega t/\gamma)$$

Injecting this particular solution in (1)-(2) leads to the following system

$$\begin{cases} -\mathrm{i}\omega\widehat{n}_{1,\ell} - \mathrm{i}\ell\dfrac{\partial_r n_0}{r}\widehat{\Phi}_{1,\ell} + \mathrm{i}\ell\dfrac{\partial_r\Phi_0}{r}\widehat{n}_{1,\ell} = 0, \\ -\partial_r^2\widehat{\Phi}_{1,\ell} - \dfrac{\partial_r\widehat{\Phi}_{1,\ell}}{r} + \dfrac{\ell^2}{r^2}\widehat{\Phi}_{1,\ell} = \widehat{n}_{1,\ell}. \end{cases} \tag{5}$$

We express $\widehat{n}_{1,\ell}$ in terms of $\widehat{\Phi}_{1,\ell}$ to get an equation on $\widehat{\Phi}_{1,\ell}$:

$$\left(-\mathrm{i}\omega + \mathrm{i}\ell\frac{\partial_r\Phi_0}{r}\right)(-\partial_r^2\widehat{\Phi}_{1,\ell} - \frac{\partial_r\widehat{\Phi}_{1,\ell}}{r} + \frac{\ell^2}{r^2}\widehat{\Phi}_{1,\ell}) = \mathrm{i}\ell\frac{\partial_r n_0}{r}\widehat{\Phi}_{1,\ell}, \tag{6}$$

We can proceed in the numerical resolution of the problem by making a discretization in the radial direction. With a uniform radial mesh $r_i = r_{\min} + i\Delta r$, $\Delta r = (r_{\max} - r_{\min})/N$ and $N \in \mathbb{N}^*$, we introduce the following notations and approximations

$$\widehat{\Phi}_{1,\ell}(r_i) = \phi_i,$$
$$\partial_r\widehat{\Phi}_{1,\ell}(r_i) = \frac{\phi_{i+1} - \phi_{i-1}}{2\Delta r},$$
$$\partial_r^2\widehat{\Phi}_{1,\ell}(r_i) = \frac{\phi_{i+1} - 2\phi_i + \phi_{i-1}}{\Delta r^2}.$$

Then, (6) is approximated by $A\phi = cB\phi$, with $c = \omega/\ell$ and where $\phi = (\phi_0, \phi_1, \ldots, \phi_N)^T \in \mathbb{R}^{N+1}$ and A, B are two matrices of size $N+1$. The problem is then reduced to find the eigenvalues c of the problem $B^{-1}A\phi = c\phi$. For each ℓ, we look for the eigenvalue c which has the greatest (strictly positive) imaginary part. We refer to [7], [13] for more details.

Analytical growth rates $|\Im(\omega)|$ of the linear phase are obtained for all the discussed boundary conditions and comparison is made with BSL method on 128×128 grid, $\Delta t = 0.05$, $r_{\min} = 1$, $r_{\max} = 10$, $\gamma = 1$. In the following tables, comparisons between analytical and numerical growth rate for different modes ℓ and different $r^{\pm}$ are performed

- Table 1 refers to the first case (homogeneous Dirichlet boundary condition).
- Table 2 refers to the second case (Neumann mode 0).
- Table 3 refers to the third case (homogeneous Neumann boundary condition).

One can observe that the numerical instability rates are very close to the analytical ones (relative error of about 0.1%).

On Fig. 1 and 2, the time history of the electric energy and of the total mass is plotted considering different boundary conditions, and for different number of points and time step. The influence of the boundary conditions on the conservation of $\mathcal{E}(t)$ and $\mathcal{M}(t)$ is confirmed numerically since in the third case (homogeneous Neumann), these two quantities are not preserved with time. On the contrary, with the same numerical parameter, the use of Neumann mode 0 leads to a very good conservation.

ℓ	r^-	r^+	$\Im(\omega)$	analytical
2	4	5	0.2875, $t \in [26, 55]$	0.288739227554270
3	4	5	0.3667, $t \in [26, 72]$	0.367315895142460
4	4	5	0.3852, $t \in [26, 51]$	0.384081542249742
7	6	7	0.3424, $t \in [26, 61]$	0.337573424025866

Table 1. Growth rate obtained by the semi-Lagrangian method and by the linearized analysis with homogeneous Dirichlet boundary conditions.

ℓ	r^-	r^+	$\Im(\omega)$	analytical
2	4	5	0.0719, $t \in [93, 138]$	0.0717643545314240
3	4	5	0.2264, $t \in [33, 87]$	0.226724091815516
4	4	5	0.2991, $t \in [34, 69]$	0.298891133128847
7	6	7	0.3338, $t \in [35, 53]$	0.330764942142169

Table 2. Growth rate obtained by the semi-Lagrangian method and by the linearized analysis with Neumann for mode 0 boundary conditions.

ℓ	r^-	r^+	$\Im(\omega)$	analytical
2	4	5	0.0672, $t \in [89, 151]$	0.067338570606553
3	4	5	0.2263, $t \in [32, 89]$	0.226665019518819
4	4	5	0.2991, $t \in [34, 69]$	0.298891598934172
7	6	7	0.3338, $t \in [35, 53]$	0.330764942148054

Table 3. Growth rate obtained by the semi-Lagrangian method and by the linearized analysis with Neumann boundary conditions.

3 Drift-kinetic Vlasov equation

In this section, we look for $f = f(t, r, \theta, z, v)$ satisfying the following $4D$ slab drift-kinetic equation (see [10])

$$\partial_t f - \frac{\partial_\theta\phi}{r}\partial_r f + \frac{\partial_r\phi}{r}\partial_\theta f + v\partial_z f - \partial_z\phi\partial_v f = 0, \tag{7}$$

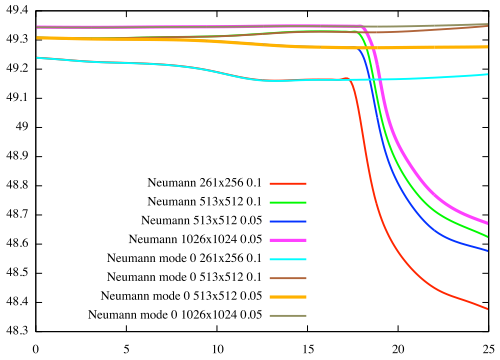

Fig. 1. Time evolution of $\mathcal{E}(t)$ for different grid sizes and Δt: study of the influence of the radial boundary conditions.

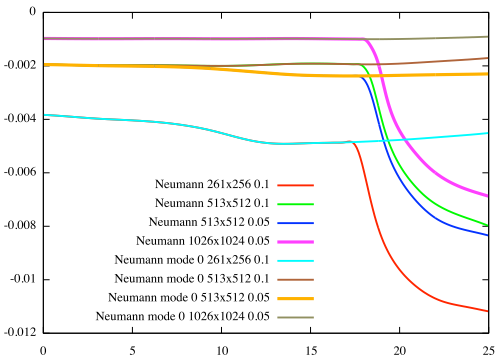

Fig. 2. Time evolution of $\mathcal{M}(t)$ for different grid sizes and Δt: study of the influence of the radial boundary conditions.

for $(r,\theta,z,v) \in \Omega \times [0,L] \times \mathbb{R}$. The self-consistent potential $\phi = \phi(r,\theta,z)$ solves the quasi neutrality equation

$$-\left[\partial_r^2\phi + \left(\frac{1}{r} + \frac{\partial_r n_0(r)}{n_0(r)}\right)\partial_r\phi + \frac{1}{r^2}\partial_\theta^2\phi\right] + \frac{1}{T_e(r)}(\phi - \langle\phi\rangle) = \frac{1}{n_0(r)}\int_{\mathbb{R}} f dv - 1, \quad (8)$$

with $\langle\phi\rangle = \frac{1}{L}\int_0^L \phi(r,\theta,z)dz$. Periodic boundary conditions are considered in the θ and z directions whereas in the radial direction, Neumann mode 0 is imposed. For the solution f, periodic boundary conditions are imposed in the θ, z, v directions, whereas in the radial r directions, Dirichlet boundary conditions are considered.

The initial function is given by

$$f(t=0,r,\theta,z,v) = f_{\rm eq}(r,v)\left[1 + \epsilon\exp\left(-\frac{(r-r_p)^2}{\delta r}\right)\cos\left(\frac{2\pi n}{L}z + m\theta\right)\right],$$

where the equilibrium function is

$$f_{\rm eq}(r,v) = \frac{n_0(r)\exp(-\frac{v^2}{2T_i(r)})}{(2\pi T_i(r))^{1/2}}.$$

The radial profiles $\{T_i, T_e, n_0\}$ have here analytical expressions

$$\mathcal{P}(r) = C_{\mathcal{P}}\exp\left(-\kappa_{\mathcal{P}}\delta r_{\mathcal{P}}\tanh(\frac{r-r_p}{\delta r_{\mathcal{P}}})\right),\ \mathcal{P} \in \{T_i, T_e, n_0\},$$

where the constants are

$$C_{T_i} = C_{T_e} = 1,\ C_{n_0} = \frac{r_{\max} - r_{\min}}{\int_{r_{\min}}^{r_{\max}} \exp(-\kappa_{n_0}\delta r_{n_0}\tanh(\frac{r-r_p}{\delta r_{n_0}}))dr}.$$

Finally, we consider the parameters of [4] (MEDIUM case)

$$r_{\min} = 0.1,\ r_{\max} = 14.5,$$
$$\kappa_{n_0} = 0.055,\ \kappa_{T_i} = \kappa_{T_e} = 0.27586,$$
$$\delta r_{T_i} = \delta r_{T_e} = \frac{\delta r_{n_0}}{2} = 1.45,\ \epsilon = 10^{-6},\ n = 1,\ m = 5,$$
$$L = 1506.759067,\ r_p = \frac{r_{\min} + r_{\max}}{2}, \delta r = \frac{4\delta r_{n_0}}{\delta r_{T_i}}.$$

4 Numerical methods

In this section, we recall the main step of the standard semi-Lagrangian method (BSL) and present a new conservative semi-Lagrangian method (CSL) in the cartesian case. The two methods bear some similarities when the $4D$ drift-kinetic model is aimed, but we detail first the two methods in a $2D$ cartesian case. A subsection will detail the modifications to deal with polar coordinates and finally the global algorithm will be presented.

We then consider a $2D$ advection equation of the form

$$\partial_t f + U(x,y)\cdot\nabla_{x,y} f = 0, (x,y) \in [0,L_x]\times[0,L_y], \quad (9)$$

where the divergence free vector field is

$$U(x,y) = (U_x(x,y), U_y(x,y)),$$

and we consider an initial condition $f(t=0,x,y) = f_0(x,y)$. We first define a spatial uniform mesh $x_i = i\Delta x$, $\Delta x = L_x/N_x$, $y_j = j\Delta y$, $\Delta y = L_y/N_y$, and a time discretization $t^n = n\Delta t$ with $n \in \mathbb{N}, \Delta t > 0$. Then, for all (x_i, y_j), we define the characteristics equation with $X(t) := (x,y)(t)$

$$\dot{X}(t) = U(X(t)),\ \ X(t^{n+1}) = (x_i, y_j),\ \ t \in [t^n, t^{n+1}]. \quad (10)$$

Let us denote by $X(s; t^{n+1}, (x_i, y_j))$ the solution of this differential system, for $s \in [t^n, t^{n+1}]$.

4.1 Standard numerical method

We recall the main steps of the $2D$ semi-Lagrangian method proposed in [17].

To go from a known function $f_{i,j}^n$ on the $2D$ mesh (x_i, y_j) to $f_{i,j}^{n+1}$, the semi-Lagrangian is based on the property that the solution is constant along the characteristics, and can be written as follows

– compute the feet of the characteristics $X(t^n;t^{n+1},(x_i,y_j))$ solution of (10)
– compute

$$f_{i,j}^{n+1} = f^n(X(t^n;t^{n+1},(x_i,y_j))),$$
$$\simeq \mathcal{I}(f^n)(X(t^n;t^{n+1},(x_i,y_j)))$$

where $\mathcal{I}$ is an interpolation operator (cubic splines for example) since $X(t^n;t^{n+1},(x_i,y_j))$ does not coincide with (x_i,y_j) in general.

4.2 A new $2D$ conservative method

In this subsection, a new conservative semi-Lagrangian is proposed. As in the finite volumes context, the unknown in this case are not point wise values but cell average values. Let us introduce a control volume $A_{i,j} = [x_{i-1/2}, x_{i+1/2}] \times [y_{j-1/2}, y_{j+1/2}]$, with $x_{i\pm1/2} = x_i \pm \Delta x/2$ and $y_{j\pm1/2} = y_j \pm \Delta y/2$ we define the unknown as

$$\bar{f}(t)_{i,j} = \frac{1}{\Delta x \Delta y}\int_{A_{i,j}} f(t,x,y)dxdy.$$

We use the fact that the volume is preserved with time. In particular, between times t^n and t^{n+1}, we get

$$(\bar{f}_{i,j}^{n+1} =) \ \frac{1}{\Delta x\Delta y}\int_{A_{i,j}} f^{n+1}(x,y)dxdy$$
$$= \frac{1}{\Delta x\Delta y}\int_{X(t^n;t^{n+1},A_{i,j})} f^n(x,y)dxdy, \quad (11)$$

where $X(t^n;t^{n+1},A_{i,j}) = \big\{X(t^n;t^{n+1},(x,y)),(x,y)\in A_{i,j}\big\}$, $X(t^n;t^{n+1},(x,y))$ being the solution at time t^n of the following characteristics equation

$$\dot{X}(t) = U(X(t)), \quad X(t^{n+1}) = (x,y)\in A_{i,j}, \quad t\in[t^n,t^{n+1}].$$

Since $\bar{f}_{i,j}^n$ is known $\forall i,j$ of the mesh, we can reconstruct a piecewise polynomial function $\mathcal{P}_{i,j}$; an example can be the Lagrange reconstruction which satisfies, $\forall i,j$

$$\frac{1}{\Delta x\Delta y}\int_{A_{i+\ell,j+k}} \mathcal{P}_{i,j}(x,y)dxdy = \bar{f}_{i+\ell,j+k}^n, \forall \ell,k = -d,\dots,d,$$

where d determines the order of the reconstruction ($\mathcal{P}_{i,j}$ is of degree $2d$ in this case).
Another example of reconstruction we propose in this work is based on Hermite reconstruction. Let us introduce some notations. First, we introduce edge average values

$$f_{i^\pm,j}^n \simeq \frac{1}{\Delta y}\int_{y_{j-1/2}}^{y_{j+1/2}} f^n(x_{i\pm1/2},y)dy,$$
$$f_{i,j^\pm}^n \simeq \frac{1}{\Delta x}\int_{x_{i-1/2}}^{x_{i+1/2}} f^n(x,y_{j\pm1/2})dx$$

and pointwise values

$$f_{i^\pm,j^\pm}^n \simeq f^n(x_{i\pm1/2},y_{j\pm1/2}).$$

We need to express these quantity as a function of the known values $\bar{f}_{i,j}^n$. For this, we first compute the edge values of the form

$$f_{i^\pm,j}^n = \sum_{\ell=r^\pm}^{s^\pm} a_\ell^\pm \bar{f}_{i+\ell,j}^n, \ f_{i,j^\pm} = \sum_{\ell=r^\pm}^{s^\pm} a_\ell^\pm \bar{f}_{i,j+\ell}^n,$$

and then the pointwise values

$$f_{i^\pm,j^\pm}^n = \sum_{\ell=r^\pm}^{s^\pm} a_\ell^\pm \bar{f}_{i+\ell,j^\pm}^n = \sum_{\ell=r^\pm}^{s^\pm} a_\ell^\pm \bar{f}_{i^\pm,j+\ell}^n,$$

with suitable coefficients $a_\ell^\pm$, $\ell = r^\pm,\dots,s^\pm$. The integers $r^\pm, s^\pm \in \mathbb{Z}$ are generally linked to the degree of approximation.

Now, for given values of $r^-\le 0$, $s^-\ge 0$, we can compute coefficients a_ℓ^-, $\ell = r^-,\dots,s^-$ in the following way. We take

$$a_\ell^- = -\sum_{k=r^-}^{\ell} \frac{\prod_{j=r^-,\ j\notin\{0,k\}}^{s^-+1}(-j)}{\prod_{j=r^-,\ j\neq k}^{s^-+1}(k-j)}, \ \ell = r^-,\dots,-1,$$

and

$$a_\ell^- = \sum_{k=\ell+1}^{s^-+1} \frac{\prod_{j=r^-,\ j\notin\{0,k\}}^{s^-+1}(-j)}{\prod_{j=r^-,\ j\neq k}^{s^-+1}(k-j)}, \ \ell = 0,\dots,s^-.$$

In a similar way, for given values of $r^+\le 0$, $s^+\ge 0$, the coefficients a_ℓ^+ are given by (for $\ell = r^+,\dots,s^+$)

$$a_\ell^+ = -\sum_{k=r^+-1}^{\ell-1} \frac{\prod_{j=r^+-1,\ j\notin\{0,k\}}^{s^+}(-j)}{\prod_{j=r^+-1,\ j\neq k}^{s^+}(k-j)}, \ \ell = r^+,\dots,0,$$

and

$$a_\ell^+ = \sum_{k=\ell}^{s^+} \frac{\prod_{j=r^+-1,\ j\notin\{0,k\}}^{s^+}(-j)}{\prod_{j=r^+-1,\ j\neq k}^{s^+}(k-j)}, \ \ell = 1,\dots,s^+.$$

For $p\in\mathbb{N}^*$, we will take

$$r^- = -\lfloor\frac{p}{2}\rfloor, \ r^+ = -\lfloor\frac{p-1}{2}\rfloor, \ s^- = \lfloor\frac{p-1}{2}\rfloor, \ s^+ = \lfloor\frac{p}{2}\rfloor.$$

Using all these expressions, we then can have an approximation

$$f_{i,j}^n(u,v) \simeq f^n(x_{i-1/2}+u\Delta x, y_{j-1/2}+v\Delta y), \text{ for } 0\le u,v\le 1.$$

For this, we can compute intermediate values

$$f_i^n(u,j^\pm) \simeq f^n(x_{i-1/2}+u\Delta x, y_{j\pm1/2}),$$
$$f_i^n(u,j) \simeq \frac{1}{\Delta y}\int_{y_{j-1/2}}^{y_{j+1/2}} f^n(x_{i-1/2}+u\Delta x,y)dy,$$

which reads, for $k\in\{j^\pm,j\}$

$$f_i^n(u,k) =$$
$$f_{i^-,k}^n + u(f_{i^+,k}^n - f_{i^-,k}^n) + u(1-u)(6f_{i,k}^n - 3(f_{i^+,k}^n + f_{i^-,k}^n)).$$

We then obtain the $2D$ reconstruction for $0 \leq u, v \leq 1$

$$f_{i,j}^n(u,v) = \\ f_i^n(u,j^-) + v(f_i^n(u,j^+) - f_i^n(u,j^-)) \\ +v(1-v)(6f_i^n(u,j) - 3(f_i^n(u,j^+) + f_i^n(u,j^-))). \quad (12)$$

Let us remark that a we start to reconstruct in the x direction but it is possible to first reconstruct in the y direction by defining $f_j^n(k,v),\ k \in \{i^\pm, i\}$ (which is the counterpart of $f_i^n(u,k), k \in \{j^\pm, j\}$).
For each choice of p, a specific Hermite method is deduced. Among them, we distinguish odd and even values of p. In (12), we can observe that if p is odd, $r^\pm = -s^\pm$ so that the reconstruction is continuous: this corresponds to PPM type reconstruction (see [3], [6]). If p is even, the reconstruction is no longer continuous since $r^\pm \neq -s^\pm$: this corresponds to LAGH type reconstruction. We refer to [9], [5] for more details.

The computation of $X(t^n; t^{n+1}, A_{i,j})$ needs some details since it is not possible to compute exactly this volume. In practice, we only compute the feet of the characteristics ending at the 4 corners of the cell $A_{i,j}$: $(x_{i\pm1/2}, y_{j-1/2})$ and $(x_{i\pm1/2}, y_{j+1/2})$. This is done by computing $X(t^n; t^{n+1}, (x_i, y_j))$ and $X(t^n; t^{n+1}, (x_{i\pm1/2}, y_{j\pm1/2}))$ is deduced by interpolation. Hence, the computation of the feet of the characteristics is performed as in the standard semi-Lagrangian method. This determines a quadrilateral volume $a_{i,j} \approx X(t^n; t^{n+1}, A_{i,j})$ which will be supposed to be convex. This can be ensured provided that the time step Δt is small enough.

The main step consists in the mesh intersection between the Lagrangian et Eulerian meshes. This step is not detailed here but we referred to [9].

The last step is the reconstruction step. Considering $a_{i,j} = \cup_{k,\ell=1} a_{i,j}^{k,\ell}$ where $a_{i,j}^{k,\ell} = a_{i,j} \cap A_{k,\ell}$, we rewrite (11) as

$$\begin{aligned} \bar{f}_{i,j}^{n+1} &= \frac{1}{\Delta x \Delta y} \int_{X(t^n;t^{n+1},A_{i,j})} f^n(x,y)dxdy, \\ &= \frac{1}{\Delta x \Delta y} \int_{a_{i,j}} f^n(x,y)dxdy, \\ &= \frac{1}{\Delta x \Delta y} \sum_{k,\ell} \int_{a_{i,j}^{k,\ell}} f^n(x,y)dxdy. \end{aligned} \quad (13)$$

From this last expression, we apply the Green theorem which reformulates a integral on a volume in an integral on segments. Then,

$$\frac{1}{\Delta x \Delta y} \sum_{k,\ell} \int_{a_{i,j}^{k,\ell}} f^n(x,y)dxdy = \\ \int_{\partial a_{i,j}^{k,\ell}} [P(x,y)dx + Q(x,y)dy],$$

where $\partial a_{i,j}^{k,\ell}$ denotes the boundary (which is composed of edges) of $a_{i,j}^{k,\ell}$ and P, Q satisfy

$$-\partial_y P(x,y) + \partial_x Q(x,y) = f^n(x,y).$$

Finally, once the piecewise polynomial function has been determined (as detailed previously), one can write, since on the subcell $a_{i,j}^{k,\ell}$ we have $f^n(x,y) = f_{k,\ell}^n(x,y)$ is approximated by a polynomial function like (12)

$$f_{k,\ell}^n(x,y) = \sum_{p,q} c_{k,\ell}^{(p,q)} x^p y^q, \ \ \forall (x,y) \in A_{i,j},$$

so that

$$\int_{a_{i,j}^{k,\ell}} f_{k,\ell}^n(x,y)dxdy = \sum_{p,q} c_{k,\ell}^{(p,q)} \int_{a_{i,j}^{k,\ell}} x^p y^q dxdy.$$

We then have to compute the integral on the right hand side. To do that, we need some notations. For each subcell $a_{i,j}^{k,\ell}$, we introduce its corners $(x_h, y_h), h = 0, \ldots, S-1$ and we suppose that $x_0 = x_S, y_0 = y_S$. Let us compute $\int_{a_{i,j}^{k,\ell}} x^p y^q dxdy$ for some given (p,q) using the Green theorem. The case $p = q = 1$ leads to

$$\begin{aligned} \int_{a_{i,j}^{k,\ell}} xydxdy &= \sum_{h=1}^{S} \int_{(x_{h-1},y_{h-1})}^{(x_h,y_h)} \frac{x^2 y}{2} dxdy \\ &= \frac{1}{2} \sum_{h=1}^{S} \int_0^1 [x_{h-1} + t(x_h - x_{h-1})]^2 \\ &\quad \times [y_{h-1} + t(y_h - y_{h-1})]\, dt\, (y_h - y_{h-1}) \\ &= \frac{(y_h - y_{h-1})}{2} \sum_{h=1}^{S} [y_{h-1}(3x_{h-1}^2 + 2x_{h-1}x_h + x_h^2) \\ &\quad + y_h(x_{h-1}^2 + 2x_{h-1}x_h + 3x_h^2)], \end{aligned}$$

where the changes of variables $x = x_{h-1} + t(x_h - x_{h-1})$ and $y = y_{h-1} + t(y_h - y_{h-1})$ have been done.

The algorithm of the conservative method to solve (9) then reads

- compute the 4 corners of $a_{i,j}$ by solving the characteristics ending at the 4 corners of $A_{i,j}$ backward in time,
- compute the intersection between the Lagrangian mesh and the cartesian axis,
- compute the corners of $a_{i,j}^{k,\ell}$ $((x_h, y_h), h = 1, \ldots, S)$,
- compute the piecewise polynomial function using a Lagrange or Hermite reconstruction,
- compute $\int_{a_{i,j}^{k,\ell}} x^p y^q dxdy$ with the Green theorem,
- compute $\bar{f}_{i,j}^{n+1}$ with (13).

4.3 Polar coordinates

The two methods have been validated in classical test cases in cartesian configurations (using Vlasov-Poisson or guiding-center models). To deal with polar coordinates and non homogeneous Dirichlet boundary conditions, some adaptations are needed, similar to techniques proposed in [11] for the FSL method.

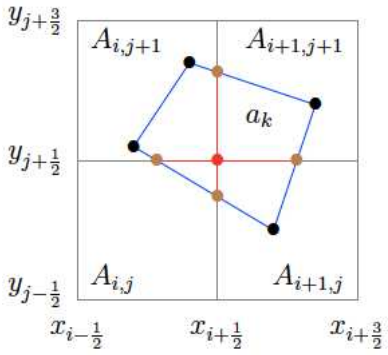

Fig. 3. Illustration of the intersection between the Lagrangian mesh $a_{k,\ell}$ and the Eulerian mesh $A_{i,j}$.

Since the new conservative method solves the conservative form of the transport equation, one has to consider the conservative solution $g(t,r,\theta) = rf(t,r,\theta)$ which is obtained by multiplying the solution by the Jacobian of the transformation. Then g solves the following conservative form

$$\partial_t g - \partial_r \left(\frac{\partial_\theta \Phi}{r} g \right) + \partial_\theta \left(\frac{\partial_r \Phi}{r} g \right) = 0. \tag{14}$$

The conservative method is then applied to this equation. Since the BSL method solves the advective form, it does not require this adaptation.

Another point concerns boundary conditions of the unknown. To overcome this delicate issue, instead of working with g, we work with the unknown $(g - g_{\text{eq}}) = r(f - f_{\text{eq}})$ which satisfies homogeneous Dirichlet boundary conditions in our applications since the solution does not depart far from the equilibrium. This is also applied to the standard BSL method.

4.4 Global algorithm

To deal with the $4D$ drift-kinetic model, a directional splitting is performed as in [10]. As said before, the standard semi-Lagrangian method and the new conservative semi-Lagrangian method have common steps, in particular because in the $1D$ z and v configuration, we deal with constant advection coefficient for which the BSL and CSL methods are equivalent (see [6]). The only difference between the two methods lies in the $2D$ advection in (r,θ). We then call BSL2D the method proposed in [10] and CSL2D the new conservative method.

The main steps of the algorithms BSL2D and CSL2D are

- solve the $1D$ advection $\partial_t f + v\partial_z f = 0$ on $\Delta t/2$ with standard semi-Lagrangian method (periodic cubic splines interpolation),
- solve $1D$ advection $\partial_t f - \partial_z \Phi \partial_v f = 0$ on $\Delta t/2$ with standard semi-Lagrangian method (periodic cubic splines interpolation),
- solve the quasi neutrality equation (8) to compute the potential Φ, with FFT in θ, z and second order finite difference in r,
- compute the derivatives $(\partial_r \Phi, \partial_\theta \Phi, \partial_z \Phi)$ of Φ with cubic splines in r, θ and second order finite differences in z,
- $2D$ advection in (r,θ) (1), with BSL or CSL,
- solve $1D$ advection $\partial_t f - \partial_z \Phi \partial_v f = 0$ on $\Delta t/2$ with standard semi-Lagrangian method (periodic cubic splines interpolation),
- solve the $1D$ advection $\partial_t f + v\partial_z f = 0$ on $\Delta t/2$ with standard semi-Lagrangian method (periodic cubic splines interpolation).

4.5 Numerical results

In this section, we compare the standard BSL method to the new conservative method. To do that, we consider the $4D$ drift-kinetic model in polar geometry (7)-(8).

We are interested in the time history of

$$\sqrt{\int \Phi^2(r_p,\theta,z) d\theta dz}, \tag{15}$$

where $r_p = (r_{\max} + r_{\min})/2$, of the total mass

$$\mathcal{M}(t) = \int_{r_{\min}}^{r_{\max}} \int_0^{2\pi} \int_0^L \int_{\mathbb{R}} f(t,r,\theta,z,v) r dv dz d\theta dr,$$

and of the total energy

$$\mathcal{E}(t) = \int_{r_{\min}}^{r_{\max}} \int_0^{2\pi} \int_0^L \int_{\mathbb{R}} \frac{v^2}{2} f(t,r,\theta,z,v) r dv dz d\theta dr + \int_{r_{\min}}^{r_{\max}} \int_0^{2\pi} \int_0^L \int_{\mathbb{R}} f(t,r,\theta,z,v) \Phi(t,r,\theta,z) r dv dz d\theta dr.$$

The first quantity (15) is known to exponentially increase in time. The growth rate can be obtained by a generalization of the approach performed in [4]. Hence, growth rates obtained in [4] can be compared to numerical results. The total mass $\mathcal{M}(t)$ is preserved by the model and it is an important point for the methods to preserve this quantity as much as possible.

In Fig. 4, we plot the time history of (15) obtained with BSL2D and CSL2D. Different variants of CSL2D method are shown, corresponding to different reconstructions presented in subsection 4.2: $p = 3$ which corresponds to third order Lagrange reconstruction, $p = 4$ (resp. 6) which corresponds to PPM (resp. PPM2), $p = 17$ which corresponds to LAGH17, and Lauritzen which corresponds to the reconstruction proposed in [12]. One can observe that the linear part is well reproduced by all the method since the instability rate of all the methods is very close to the analytical one proposed by [4].

In Fig. 5, the time history of the total mass $\mathcal{M}(t)$ (which is theoretically preserved with time) is plotted for the different methods (BSL2D and CSL2D for different reconstructions). The final time is 8000 so that the linear theory is not available any more. We can first observe that up to time 3000, the total mass is well preserved by all the methods. This time interval corresponds to the linear

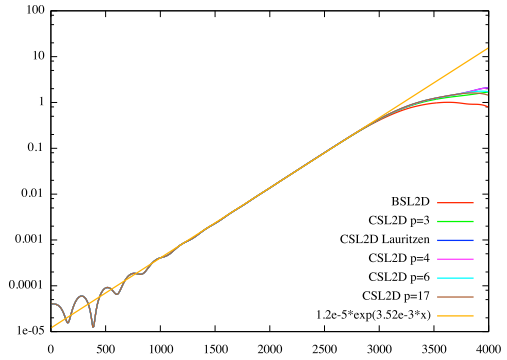

Fig. 4. Time evolution of $\sqrt{\int \Phi^2(r_p,\theta,z)d\theta dz}$ on $32\times32\times32\times64$ grid, with $\Delta t = 8$ and $v_{\max} = 7.32$.

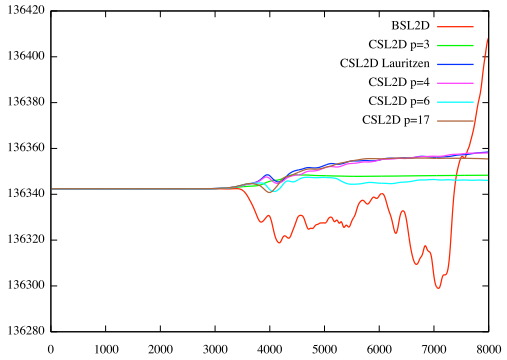

Fig. 5. Time evolution of the total mass on $32\times32\times32\times64$ grid, with $\Delta t = 8$ and $v_{\max} = 7.32$.

phase in which few occurs. After that time, the methods behave differently. In particular, BSL2D looses the conservation of the total mass (even if the relative error of about 0.1%). On the other side, CSL2D presents a better behavior (relative error of about 0.01%). Among the different reconstructions, CSL2D $p = 6$ (which corresponds to PPM2) behaves in the best way.

Fig. 6 shows the time history of $\mathcal{E}(t)$ (which is theoretically preserved with time) obtained with the different methods. This invariant is quite difficult to preserve numerically and we can observe that, as for the total mass, the CSL methods have a very good behavior compared to the BSL method since the total energy is conserved in an better order (about 0.1% for CSL and about 1% for BSL). One interesting point is the very similar behavior of the total mass and total energy. It seems that the loss of the mass conservation has a strong influence on the total energy conservation. Obviously we have to go further into the comparisons but these first results are quite promising.

5 Conclusion/ future work

In this work, we proposed two non trivial test cases in polar geometry and a new conservative semi-Lagrangian

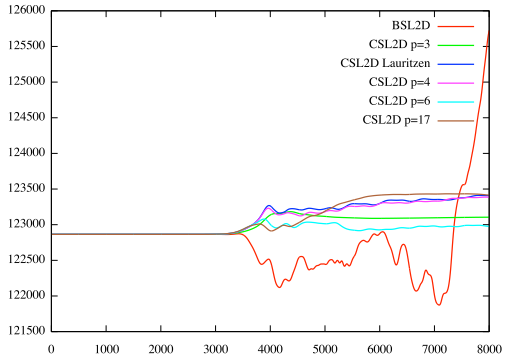

Fig. 6. Time evolution of the total energy on $32\times32\times32\times64$ grid, with $\Delta t = 8$ and $v_{\max} = 7.32$.

method. The first test concerns a guiding-center model for which boundary conditions in the radial directions are discussed. It appears that some good choices leads to conservation of electric energy and total mass. This is confirmed by the numeric results. The second test concerns a $4D$ drift-kinetic model which can be viewed as a first step to describe tokamak plasmas. For these two models, a linear analysis can be performed and instability rates can be obtained to validate the numerical methods in the linear phase.

For this latter case, we propose and validate a new conservative semi-Lagrangian method. This method seems to be a good alternative to the standard pointwise semi-Lagrangian method which is not conservative in this configuration. More comparisons are performed in [9] and [5] in this two intermediate configurations (guiding-center and $4D$ drift-kinetic) to confirm the good behavior of the conservative semi-Lagrangian method.

References

1. C.K. Birdsall, A.B. Langdon, *Plasma Physics via Computer Simulation*, Inst. of Phys. Publishing, Bristol/Philadelphia, 1991.
2. C.Z. Cheng, G. Knorr, *The integration of the Vlasov equation in configuration space*, J. Comput. Phys. 22, (1976), pp. 330-3351.
3. P. Colella, P. Woodward, *The Piecewise Parabolic Method (PPM) for gas-dynamical simulations*, J. Comput. Phys. 54, (1984), pp. 174-201.
4. D. Coulette, N. Besse, *Numerical comparisons of gyrokinetic multi-water-bag models*, J. Comput. Phys. 248, (2013), pp. 1-32.
5. N. Crouseilles, P. Glanc, M. Mehrenberger, $2D$ *advective and conservative semi-Lagrangian schemes upwind Hermite type reconstruction*, in preparation.
6. N. Crouseilles, M. Mehrenberger, E. Sonnendrücker, *Conservative semi-Lagrangian method for the Vlasov equation*, J. Comput. Phys. 229, (2010), pp. 1927-1953.
7. R.C. Davidson, *Physics of non neutral plasmas*, Addison-Wesley, Redwood City, CA,1990.

8. R. Gagné, M. Shoucri, *A splitting scheme for the numerical solution of a one-dimensional Vlasov equation*, J. Comput. Phys. 24, (1977), pp. 445-449.
9. P. Glanc, *Approximation numérique de lquation de Vlasov par des méthodes de type remapping conservatif*, PhD of the University of Strasbourg, 2014.
10. V. Grandgirard, M. Brunetti, P. Bertrand, N. Besse, X. Garbet, P. Ghendrih, G. Manfredi, Y. Sarazin, O. Sauter, E. Sonnendrücker, J. Vaclavik, L. Villard, *A drift-kinetic Semi-Lagrangian 4D code for ion turbulence simulation*, J. Comput. Phys. 217, (2006), pp. 395-423.
11. G. Latu, V. Grandgirard, J. Abiteboul, M. Bergot, N. Crouseilles, X. Garbet, P. Ghendrih, M. Mehrenberger, Y. Sarazin, H. Sellama, E. Sonnendrücker, D. Zarzoso, *Accuracy of unperturbed motion of particles in a gyrokinetic semi-Lagrangian code*, INRIA Research Report 8054.
12. P. Lauritzen, D. Ramachandran, P. Ullrich, *A conservative semi-Lagrangian multi-tracer transport scheme (CSLAM) on the cubed-sphere grid*, J. Comput. Phys. 229, (2010), pp. 1401-1424.
13. E. Madaule, S. Hirstoaga, M. Mehrenberger, J. Pétri, *Semi-Lagrangian simulations of the diocotron instability*, hal-00841504.
14. J. Pétri, *The diocotron instability in a pulsar "cylindrical" electrosphere*, Astronomy & Astrophysics, 2008.
15. J. Pétri, *Non-linear evolution of the diocotron instability in a pulsar electrosphere: 2D PIC simulations*, Astronomy & Astrophysics, 2009.
16. SELALIB, http://selalib.gforge.inria.fr/
17. E. Sonnendrücker, J. Roche, P. Bertrand, A. Ghizzo, *The Semi-Lagrangian Method for the Numerical Resolution of the Vlasov Equation*, J. Comput. Phys. 149, 201-220 (1999).
18. C. Yang, F. Filbet, *Conservative and non-conservative methods based on Hermite weighted essentially-non-oscillatory reconstruction for Vlasov equations*, submitted, http://arxiv.org/pdf/1312.4481v1.pdf